

Non-stationary analysis of the frequency and intensity of heavy precipitation over Canada and their relations to large-scale climate patterns

Xuezhi Tan^{1,2} · Thian Yew Gan¹

Received: 3 November 2015 / Accepted: 17 June 2016 / Published online: 24 June 2016
© Springer-Verlag Berlin Heidelberg 2016

Abstract In recent years, because the frequency and severity of floods have increased across Canada, it is important to understand the characteristics of Canadian heavy precipitation. Long-term precipitation data of 463 gauging stations of Canada were analyzed using non-stationary generalized extreme value distribution (GEV), Poisson distribution and generalized Pareto (GP) distribution. Time-varying covariates that represent large-scale climate patterns such as El Niño Southern Oscillation (ENSO), North Atlantic Oscillation (NAO), Pacific decadal oscillation (PDO) and North Pacific Oscillation (NP) were incorporated to parameters of GEV, Poisson and GP distributions. Results show that GEV distributions tend to under-estimate annual maximum daily precipitation (AMP) of western and eastern coastal regions of Canada, compared to GP distributions. Poisson regressions show that temporal clusters of heavy precipitation events in Canada are related to large-scale climate patterns. By modeling AMP time series with non-stationary GEV and heavy precipitation with non-stationary GP distributions, it is evident that AMP and heavy precipitation of Canada show strong non-stationarities (abrupt and slowly varying changes) likely because of the influence of large-scale climate patterns. AMP in southwestern coastal regions, southern Canadian Prairies and the Great Lakes

tend to be higher in El Niño than in La Niña years, while AMP of other regions of Canada tends to be lower in El Niño than in La Niña years. The influence of ENSO on heavy precipitation was spatially consistent but stronger than on AMP. The effect of PDO, NAO and NP on extreme precipitation is also statistically significant at some stations across Canada.

Keywords Canadian extreme precipitation · Non-stationary probability distributions · Poisson regression · Climate indices · Trend · El Niño Southern Oscillation · Large-scale climate patterns

1 Introduction

In recent decades, Canada have experienced extreme flood events such as the Saint John River flood in 2008 (Newton and Burrell 2015), the Red River Flood in 2009 (Wazney and Clark 2015) and 2011 (Stadnyk et al. 2015), the South Saskatchewan and Elk River flood in 2013 (Pomeroy et al. 2015), the Assiniboine River flood in 2011 (Blais et al. 2015) and 2014 (Ahmari et al. 2015), the Richelieu River flood in 2011 (Saad et al. 2015), the southern Alberta flood in 2013 (Milrad et al. 2015), and the Southeastern Canadian Prairies (CP, which consists of Alberta, Saskatchewan and Manitoba) flood in 2014 (Szeto et al. 2015). These extreme flood events have caused substantial damage to Canada, such as damage to infrastructure, financial losses, and even loss of human life. For instance, the total damage of the June, 2013 flood of southern Alberta is estimated at \$5–6 billion, making it the costliest natural disaster in Canadian history (Environment Canada 2014; Government of Alberta 2014).

For large river basins of Canada, floods are often associated with spring snowmelt, rain-on-snow, or

Electronic supplementary material The online version of this article (doi:10.1007/s00382-016-3246-9) contains supplementary material, which is available to authorized users.

✉ Thian Yew Gan
tgan@ualberta.ca

¹ Department of Civil and Environmental Engineering, University of Alberta, Edmonton, AB T6G 2W2, Canada

² State Key Laboratory of Water Resources and Hydropower Engineering Science, Wuhan University, Wuhan, China

long-duration heavy precipitation with large areal coverage, even though the significance of heavy rainstorms and snowstorms that resulted in floods varies across the country (Buttle et al. 2016). Because Canada is seasonally covered with snow, floods related to spring snowmelt or rain-on-snow events are common in Canada. In southern Canada, convective and frontal systems can give rise to long-duration heavy, summer rainfall events that trigger floods in large river basins, or intensive, short-duration storms which can also trigger floods in small to medium river basins.

Changes to Canadian extreme and heavy precipitation under the global warming impact can increase the risk of flooding. Climate warming due to increasing atmospheric greenhouse gasses can intensify the hydrologic cycle (Seager et al. 2012). For example, according to the Clausius-Clapeyron equation, the water-holding capacity of the atmosphere increases at about 7 % per K temperature rise, and so warming will increase atmospheric moisture, and so severe storms become more intensive (Allan and Soden 2008). The potential cost associated with heavy precipitation (rainfall and snowfall) for Canadian society motivates us to assess whether the frequency and intensity of extreme or heavy precipitation have changed over Canada. Therefore in this study, our specific objective is to detect possible changes in extreme and heavy precipitation over Canada: (1) temporal non-stationarities (abrupt and slowly varying changes); (2) Frequency analyses and upper tail properties of annual maximum daily precipitation (AMP); (3) Occurrences of heavy precipitation temporal clusters; and (4) Relationships between Canadian extreme and heavy precipitation and some large-scale climate patterns.

For Canada, previous studies detected overall increasing trends in the annual total precipitation in the twentieth century mostly because of the increase in small to moderate precipitation events (Mekis and Vincent 2011; Vincent and Mekis 2006; Zhang et al. 2000, 2001), while winter total snowfall has mainly increased in the north but decreased in southwestern Canada since 1950 (Mekis and Vincent 2011; Vincent and Mekis 2006). In contrast, results of past studies on the trend analysis of heavy or extreme precipitation over Canada are inconsistent in the twentieth century possibly because of different datasets or methods used. Some studies found no statistically significant trend (Kunkel 2003; Kunkel and Andsager 1999; Zhang et al. 2001; Vincent and Mekis 2006), while others detected statistically significant increasing trends (Alexander et al. 2006; Burn and Taleghani 2013; Peterson et al. 2008) in either the frequency or intensity of extreme precipitation. Some regional climate modeling studies projected more intensive and frequent daily and multi-day precipitation events in a warmer future climate for most Canadian regions (Kuo et al. 2015; Mailhot et al. 2010; Mladjic et al. 2011).

Extreme events are usually defined by the block maxima, peaks-over-threshold (POT) or point processes (Coles 2001; Khaliq et al. 2006). Compared to the block maxima approach that models extreme events using a generalized extreme value (GEV) distribution, the POT approach fits all events exceeding a specified threshold to a generalized Pareto (GP) distribution and the occurrence of an exceedance to a Poisson process. By accepting hydroclimatic processes as inherently probabilistic, a changing climate can be modeled using a non-stationary probability distribution. To avoid possible confusion about definitions regarding extremes, samples of maximum events for the block maxima method will be referred to as *extreme* events while events for the POT approach as *heavy* events.

Temporal clustering of events contributes to the non-stationarity of a time series (Franzke 2013; Mailier et al. 2006; Mallakpour and Villarini 2015; Pinto et al. 2013; Trambly et al. 2013; Villarini et al. 2011, 2013), which is often overlooked in hydroclimatic frequency analysis. If heavy events are stationary, the number of occurrences of such events follows a homogeneous Poisson distribution. However, large-scale weather patterns or other factors can affect storm tracks responsible for the occurrence of heavy events in clusters, making the homogeneous assumption invalid.

As the probability of occurrences of climate extremes can be strongly affected by large-scale climate patterns, considerable progress has been made in deriving possible relationships between such climate patterns and extreme climate variables by modeling the latter with non-stationary GEV and GP distributions using climate indices as time-varying covariates (Kenyon and Hegerl 2008). Zhang et al. (2010) fitted winter daily maximum precipitation over North America (NA) to a GEV distribution, using climate indices such as El Niño Southern Oscillation (ENSO), Pacific decadal oscillation (PDO), and North Atlantic Oscillation (NAO) as covariates for the location and/or scale parameters of the GEV distribution. They found that ENSO and PDO have spatially consistent and statistically significant influences on NA extreme winter precipitation. Sillmann et al. (2011) fitted the monthly minima of European winter 6-h minimum temperature to a GEV distribution with an indicator for atmospheric blocking conditions as a covariate to the location and scale parameters of the GEV distribution and detected the cooling effect of atmospheric blocking. Min et al. (2013) conducted a non-stationary GEV analysis of seasonal temperature and precipitation extremes over Australia, by specifying GEV parameters as linear functions of large-scale climate patterns such as ENSO, Indian Ocean Dipole, and Southern Annular Mode. Maraun et al. (2010) developed a generalized linear model to relate the influence of atmospheric circulations on extreme daily

precipitation across the UK, by incorporating synoptic scale airflow strength, direction and vorticity to the location and scale parameters of the GEV distribution. Instead of modeling winter precipitation of multiple sites in California to a GEV model separately, Shang et al. (2011) jointly modeled the winter maximum daily precipitation of 192 sites of California with spatial, max-stable process models by incorporating the Southern Oscillation Index (SOI) as a co-variate to the marginal GEV distributions of this spatial model. All these are examples on modeling recent changes in the frequency and intensity of extreme climate and weather events using non-stationary distributions. Given that no study has been conducted to model possible changes to all of Canadian extreme and heavy precipitation using non-stationary probability distributions, several non-stationary approaches were used to characterize the changing frequency and intensity of extreme and heavy precipitation over Canada and the possible influence of large-scale climate patterns on Canadian extreme and heavy precipitation.

The remainder of this paper is organized as follows: data description is given in Sect. 2, methods applied to detect nonstationarities of Canadian heavy precipitation are given in Sect. 3, discussion of results in Sect. 4, and summary and conclusions in Sect. 5.

2 Data and methods

2.1 Precipitation

The daily precipitation measurements, including total precipitation, rainfall and snowfall data used in this study were obtained from the second generation, adjusted historical Canadian climate data (AHCCD) database, which contains 463 stations (Fig. 1) of precipitation observations statistically adjusted for known measurement issues such as wind undercatch, evaporation and wetting loss for each type of rain-gauge, snow water equivalent from ruler measurements, trace observations and accumulated amounts from several days. More detailed information on this datasets is given in Mekis and Vincent (2011). Because station closures and relocation were ongoing issues, observations from some nearby stations (a total of 12.3 % of all stations) after 1990 were occasionally combined to create long-term precipitation time series for climate change studies.

AHCCD is the most homogeneous long-term measured data currently available for Canadian daily precipitation. The length of the measured daily precipitation ranges 27–172 years, with an average of 84 years. The year that precipitation measurements began in stations of northern

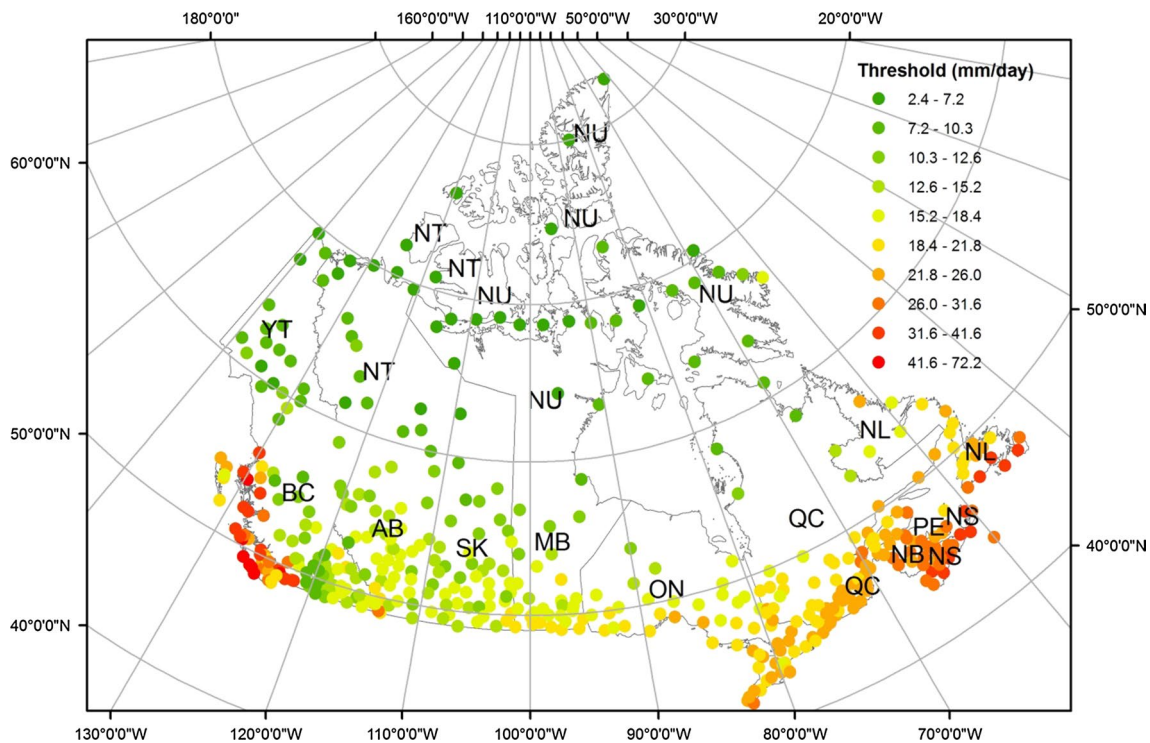


Fig. 1 Location of the 463 Canadian precipitation stations used in this study, together with the threshold values used for the POT analyzes. Province or Territories of Canada are: AB Alberta, SK Saskatchewan, MB Manitoba, NL New Founland and Labrador, PE

Prince Edward Island, NS Nova Scotia, NT Northwest Territories, NU Nunavut, ON Ontario, NB New Brunswick, YT Yukon Territory, BC British Columbia, QC Quebec

Canada is much later than southern Canada, so stations with short precipitation measurements are usually located in northern Canada. Because our objective is to investigate extreme and heavy precipitation changes over the whole country, all the second generation precipitation data from AHCCD were included for this study. To check the uncertainties of non-stationary analysis because of the inconsistent length of time series, we also analyzed data within four periods with the same non-stationary analysis. These four periods are: (1) 1900–2010 (111 years for 41 stations), (2) 1930–2010 (81 years for 140 stations), (3) 1950–2010 (61 years for 201 stations) and (4) 1970–2010 (41 years for 223 stations). However, we report results by analyzing all available data and stations, unless otherwise specified.

Since we have no knowledge of the weather condition in days without precipitation records, precipitation of these days was first replaced with 0. The annual maximum daily precipitation (AMP) was extracted from the daily time series for each station. The missing AMPs (<3 % of all the years of data for each station) were replaced with the mean value of that AMP time series excluding missing values. To extract heavy precipitation, Groisman et al. (1999) used a threshold of 25.4 mm (1 inch) in Canada, but Mekis and Hogg (1999) considered the largest 10 % of daily precipitation events as heavy precipitation events to account for substantial variations in heavy precipitation across Canada, since the mean intensity of extreme events decreases rapidly in latitudes above 50°N. For every season of each station over Canada, Zhang et al. (2001) defined the heavy precipitation by a threshold that is exceeded on an average three events per year.

For the POT analysis of this study, the 95th percentile of nonzero daily precipitation based on the precipitation empirical probability distribution is chosen as the threshold to define heavy precipitation of Canada, which was also used by Villarini et al. (2013) for distribution changes of heavy rainfall over the central United States. Across Canada, the magnitude of the 95th percentile of nonzero daily precipitation decreases from south to north with relatively high values in southwestern and eastern coastal regions (Fig. 1). Using the 95th percentile criterion, threshold values chosen for Canada range from 2 to 70 mm. Based on the threshold value for each station, the number (counts) of heavy precipitation in each year and the amount each heavy precipitation exceeded the threshold is noted.

From the spatial distribution of AMP that had occurred in each month over Canada (Fig. S1), it is clear that for the CP and northwestern Canada, AMP mainly occurred either during summer or early autumn (from June to September), more in mid-winter (January) for eastern and northern Canada (above 60°N), but almost year round in localized, southwestern and southeastern coastal areas (Fig. S1). Thus, seasonal distributions of AMP are unimodal

in southwestern Canada during summers but bimodal in northern and southeastern Canada with peaks during both summers and winters. However, heavy precipitation of Canada as defined above were more evenly distributed yearly than AMP, even though heavy precipitation events tend to occur more frequently during summer and early Autumn, and relatively infrequently during winters (Fig. S2).

2.2 Large-scale climate anomalies

We selected five large-scale climate indices that have been linked to precipitation variability over Canada (Gan et al. 2007; Shabbar et al. 1997) or over NA (Ropelewski and Halpert 1986; Zhang et al. 2010). These five climate indices are SOI (Ropelewski and Jones 1987), NINO3 (Rayner et al. 2003) which is a time series of equatorial Pacific (Niño 3 region) sea surface temperature (SST) anomalies, NAO (Hurrell and Loon 1997), PDO (Mantua et al. 1997), and North Pacific (NP) (Trenberth and Hurrell 1994) Index which is the area-weighted sea level pressure anomalies over 30°N–65°N, 160°E–140°W. SOI and NINO3 represent the ENSO phenomenon. Because many high-frequent and small-scale phenomena in the atmosphere can influence the pressures at stations (Darwin and Tahiti) involved in forming the SOI but do not reflect the ENSO itself, we also use NINO3, which is more robust to identify El Niño and La Niña events (Trenberth 1997), to represent ENSO. Monthly time series of SOI, NINO3, NAO, PDO and NP were downloaded from the Global Climate Observing System Working Group on Surface Pressure website (www.esrl.noaa.gov/psd/gcos_wgsp/Timeseries/). Time series of yearly values were derived from averaging monthly values over the entire year. We also used National Centers for Environmental Prediction/National Centre for Atmospheric Research Reanalysis 1 dataset (Kalnay et al. 1996) to estimate daily circulation patterns concerning geopotential heights, wind field and vertically integrated precipitable water content (PWC).

2.3 Research methodology

The non-stationary frequency analysis of extreme or heavy events was conducted using the non-stationary block maxima and POT approaches (Coles 2001). Block maxima of extreme precipitation events were fitted with both stationary and non-stationary GEV distributions (Appendix 1). The number of heavy precipitation events was fitted with a non-stationary Poisson distribution (Appendix 2), and exceedances of precipitation events over a threshold defined as the 95th percentile of non-zero precipitation were fitted to a non-stationary GP distribution (Appendix 3) with time-varying parameters. Trends of the intensity of extreme

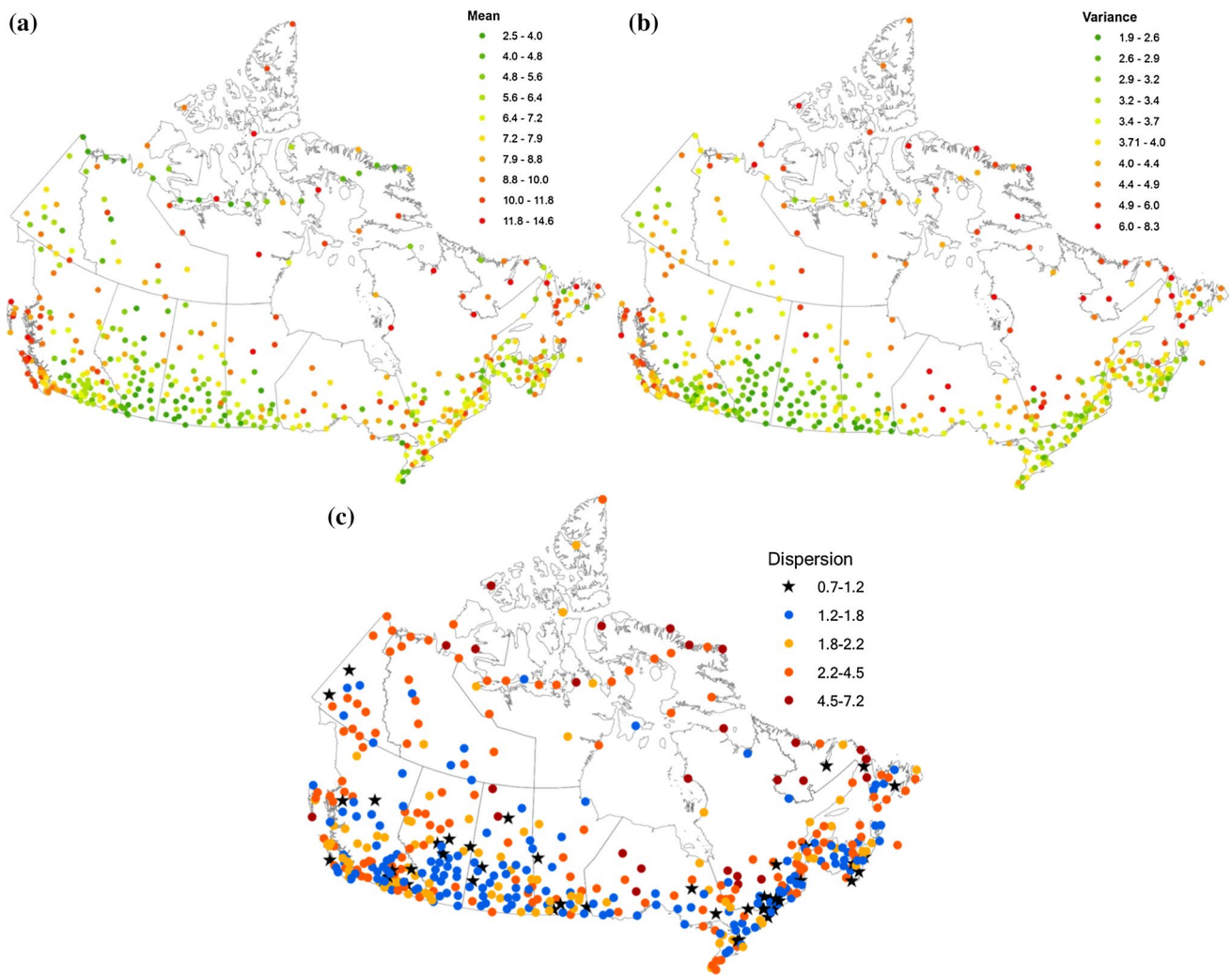


Fig. 2 Maps with the mean (a), variance (b), and dispersion coefficient (c) of the number of days exceeding corresponding 95th percentile daily precipitation. The dispersion coefficient is defined as the ratio of variance to mean

precipitation were analyzed using time as a covariate to the parameters of GEV and GP distributions. Because most heavy precipitation of Canada shows an over-dispersion behavior (see Fig. 2; Sect. 3.2), trends and change points to the number of occurrences of heavy precipitation events were modeled by a Poisson regression and a segmented regression models (Muggeo 2003; Appendix 2), respectively. We used annual time series of five climate indices, namely, SOI, NINO3, NAO, PDO and NP, as covariates of parameters of non-stationary GEV, Poisson and GP distributions to examine the influence of large-scale climate patterns on extreme and heavy precipitation over Canada. The likelihood-ratio test (Coles 2001; Appendix 4) was applied to test the significance of the relationship between parameters of distributions and covariates.

We used composite methods to assess the impact of extreme phases of ENSO, PDO, NAO and NP on Canadian

heavy precipitation. Represented by the geopotential height, wind field and PWC, composite circulation patterns associated with the 10 largest and 10 smallest values for each climate index during 1948–2010 were computed for the summer (somewhere between May and August) and winter (between October and February) when heavy precipitations are more likely to occur (Fig. S2). A systematic comparison of the composite analysis of synoptic circulation patterns that gave rise to heavy precipitation was conducted for different regions by dividing Canada into western, central and eastern Canada (Fig. 1), respectively. From the 35th to 65th percentile (30 % interval) of the empirical cumulative distribution for Julian days on which heavy precipitation most likely occurred in the summer or winter of each region, we extracted large-scale anomalies (with respect to the long-term mean of 1948–2010) of geopotential heights, wind field, and PWC for this 30 % interval

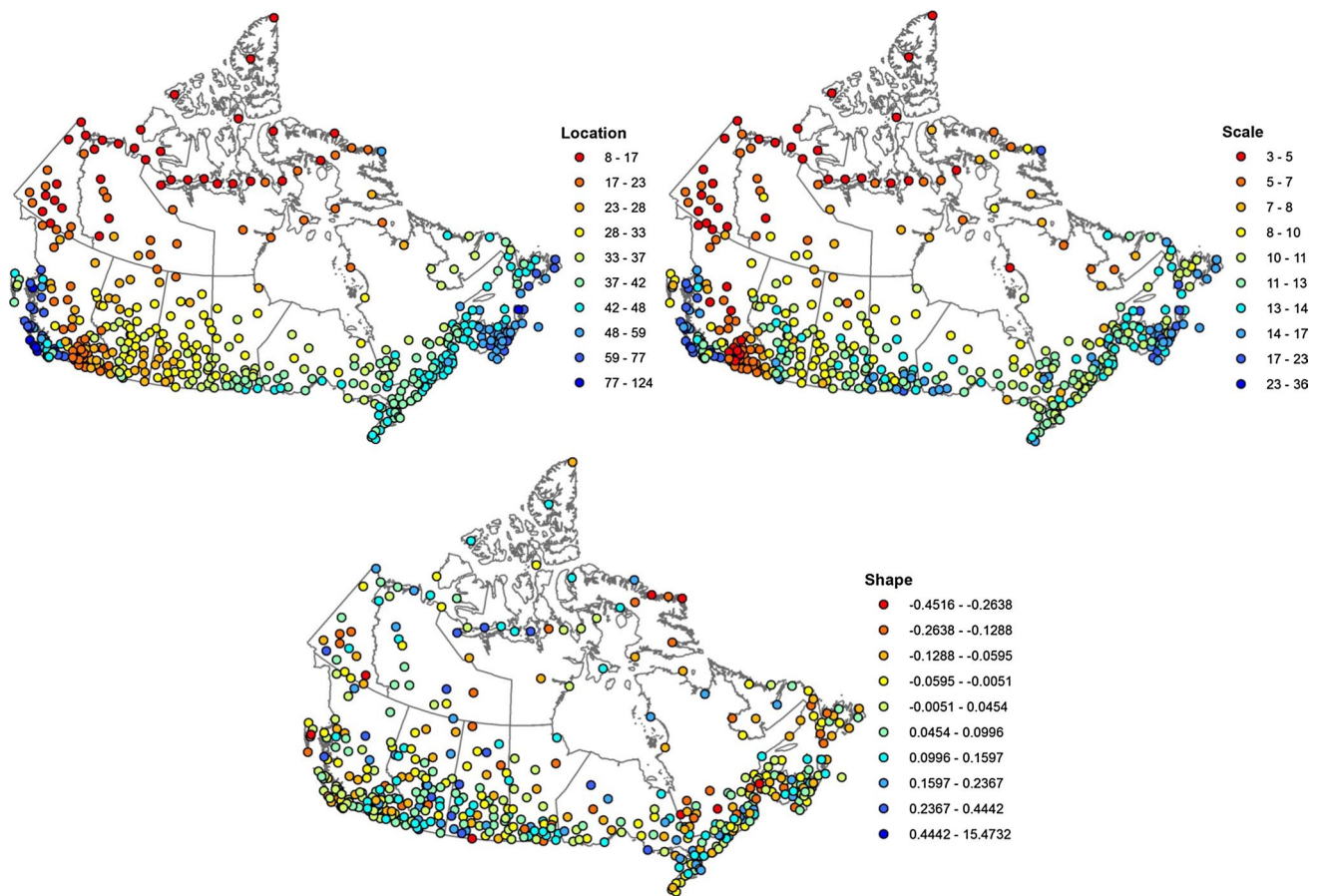


Fig. 3 Maps of location, scale and shape parameters of the GEV distribution for AMP time series derived from the stationary analysis

selected for each composite year. Composite anomalies are the mean of climate anomalies in years with extremely high and low climate indices, respectively.

3 Discussion of results

3.1 Extreme value distribution of Canadian precipitation

The Kolmogorov–Smirnov and Anderson–Darling tests were used to assess the goodness-of-fit of stationary GEV distributions applied to AMP series. Results of these two tests confirm the null hypothesis at 5 % significance level that AMP time series are sampled from stationary GEV distributions for all stations, thus justifying the assumption that AMP time series can be modeled using GEV distributions. The spatial distribution of stationary GEV parameters is shown in Fig. 3, and the spatial distribution of extreme precipitation of various return periods derived from these GEV distributions is shown in Fig. 4a–c. Overall, the location and scale parameters increase from north to south and

from inland to coastal regions of Canada, with highest location and scale parameters located in southwestern and southeastern coastal regions of Canada. However, there is no clear spatial pattern for the shape parameters. Most stations have a non-zero shape parameter, which implies that most Canadian AMP series can be modeled by GEV Type II or Type III (Appendix 1) distributions with heavy tail behavior.

Figure 5 shows stations at which the fitted GEV distribution is significantly improved statistically by incorporating climate indices as covariates for both location and scale parameters, and Table 1 lists the number of these stations. Figure 5 also shows the spatial distribution of signs (+ or –) of differences between AMPs of 20-year return period estimated from GEV distributions conditioned on positive and negative phases of selected climate patterns, while Fig. 6 shows the spatial distributions of actual differences between AMPs of 20-year return period estimated from GEV distributions conditioned on the mean of five largest positive and the mean of five largest negative phases of a given climate pattern. By modeling AMP using non-stationary GEV distributions with parameters based on time as

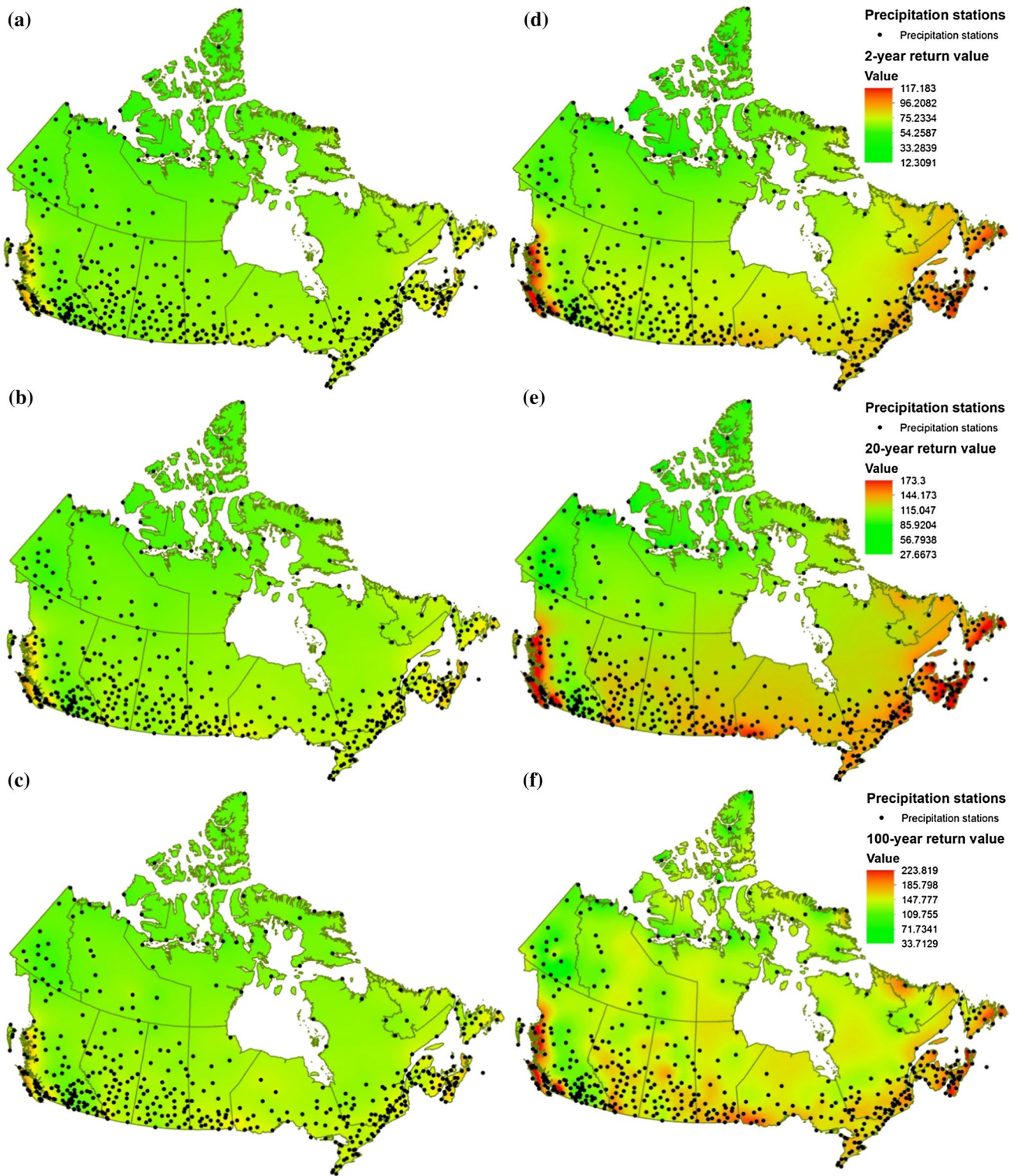


Fig. 4 Maps of AMP with the a, d 2-, b, e 20- and c, f 100-year return period derived from the stationary GEV (a–c) and GP (b–f) modeling. Spatial interpolation is performed by a simple Kriging method

the covariate, e.g., the first and the last 5-year of the study period for each station, which for the 1930–2010 period refers to 1930–1934 and 2006–2010, respectively. We have

also shown the difference in AMP estimated between the last and the first 5-year of the study period for each station. Figures 5 and 6 show that the influence of large-scale

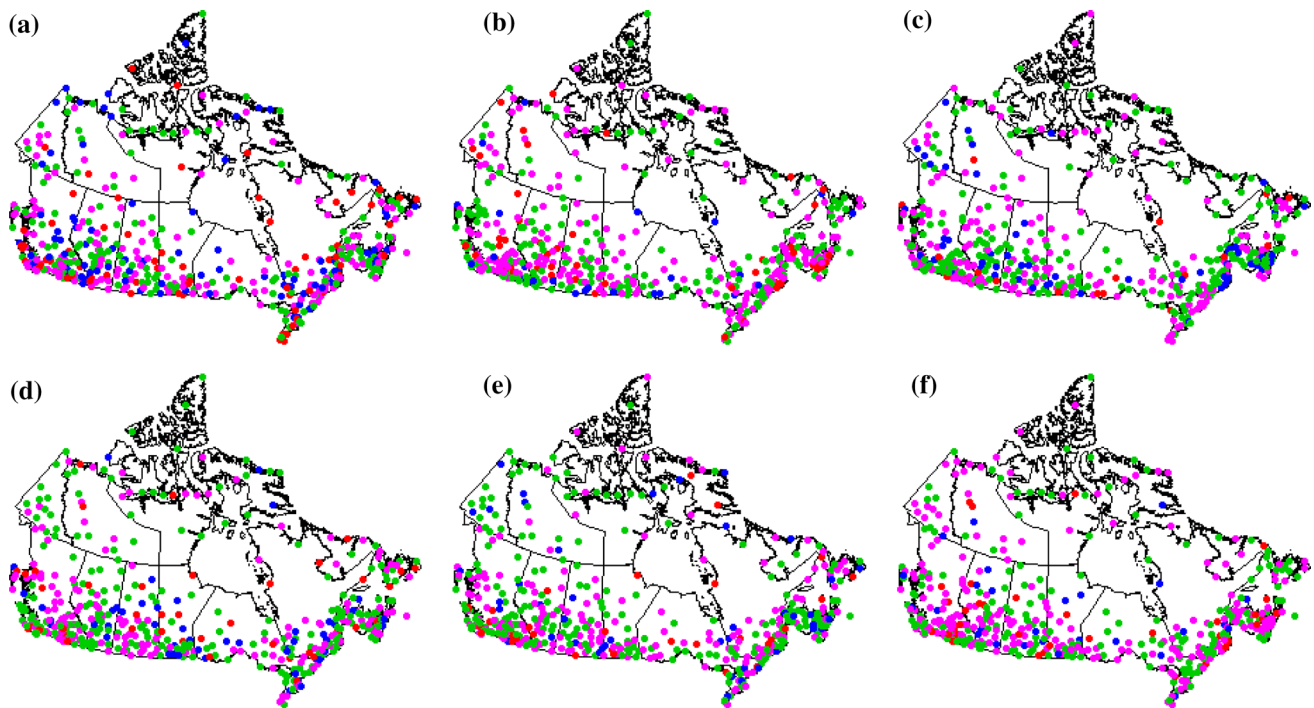


Fig. 5 Maps showing the sign of difference ($P_+[p = 0.95] - P_-[p = 0.95]$) in precipitation return levels of 20 year return period conditional on positive ($P_+[p = 0.95]$) and negative ($P_-[p = 0.95]$) phases of covariates, i.e., the time and the five selected climate indices, for the GEV models of Canadian AMP with time-varying location and scale parameters ($\mu = \beta_\mu x$ and $\log(\sigma) = \beta_\sigma x$, x is a covariate). The red and magenta dots represent the higher

AMP values in years with high values of a particular covariate ($P_+[p = 0.95] > P_-[p = 0.95]$) while the blue and green dots show the lower AMP values in years with high values of a particular covariate ($P_+[p = 0.95] < P_-[p = 0.95]$). Blue and red dots indicate stations whose GEV modeling of AMP is significantly improved by implementing the covariates at the 5% level. **a** Time (year), **b** SOI, **c** NINO3, **d** NAO, **e** PDO **f** NP

Table 1 Percentages (%) of stations where incorporating each covariate showed statistically significant improvement in the extreme precipitation modeling, compared to the stationary extreme precipitation modeling

| Periods | Probability distributions | Parameter | Time | SOI | NINO3 | NAO | PDO | NP |
|-----------|---------------------------|---------------------|------|------|-------|------|------|------|
| All data | GEV | Location | 29.4 | 10.6 | 11.5 | 14.7 | 11.7 | 14.3 |
| | GEV | Location + scale | 33.9 | 15.8 | 16.4 | 19.7 | 16.2 | 13.6 |
| | Poisson | Rate of occurrences | 66.5 | 21.8 | 21.0 | 22.5 | 30.9 | 17.7 |
| | GP | Scale | 22.3 | 10.8 | 34.3 | 11.5 | 10.8 | 35.0 |
| 1900–2010 | GEV | Location | 34.1 | 12.2 | 14.8 | 19.5 | 9.8 | 16.8 |
| | GEV | Location + scale | 31.7 | 19.8 | 17.1 | 22.0 | 14.6 | 19.8 |
| | Poisson | Rate of occurrences | 78.5 | 22.2 | 19.8 | 31.7 | 22.0 | 21.0 |
| | GP | Scale | 19.5 | 19.5 | 35.9 | 12.4 | 14.6 | 39.2 |
| 1930–2010 | GEV | Location | 19.3 | 15.0 | 15.0 | 17.9 | 10.0 | 13.4 |
| | GEV | Location + scale | 22.2 | 14.1 | 17.1 | 23.6 | 13.6 | 17.9 |
| | Poisson | Rate of occurrences | 67.8 | 17.9 | 22.9 | 22.9 | 24.3 | 27.1 |
| | GP | Scale | 16.4 | 14.3 | 44.3 | 10.7 | 12.1 | 32.9 |
| 1950–2010 | GEV | Location | 27.9 | 11.9 | 12.9 | 15.9 | 12.9 | 13.4 |
| | GEV | Location + scale | 23.4 | 15.9 | 17.4 | 18.4 | 11.9 | 10.0 |
| | Poisson | Rate of occurrences | 45.0 | 20.4 | 19.4 | 30.8 | 35.3 | 35.3 |
| | GP | Scale | 14.4 | 11.9 | 34.8 | 11.4 | 12.9 | 29.9 |
| 1970–2010 | GEV | Location | 17.9 | 15.7 | 16.1 | 14.3 | 10.8 | 13.9 |
| | GEV | Location + scale | 43.8 | 15.7 | 20.2 | 17.1 | 12.1 | 12.6 |
| | Poisson | Rate of occurrences | 55.1 | 17.1 | 17.1 | 26.5 | 20.2 | 21.5 |
| | GP | Scale | 15.2 | 13.9 | 33.6 | 11.2 | 13.9 | 24.2 |

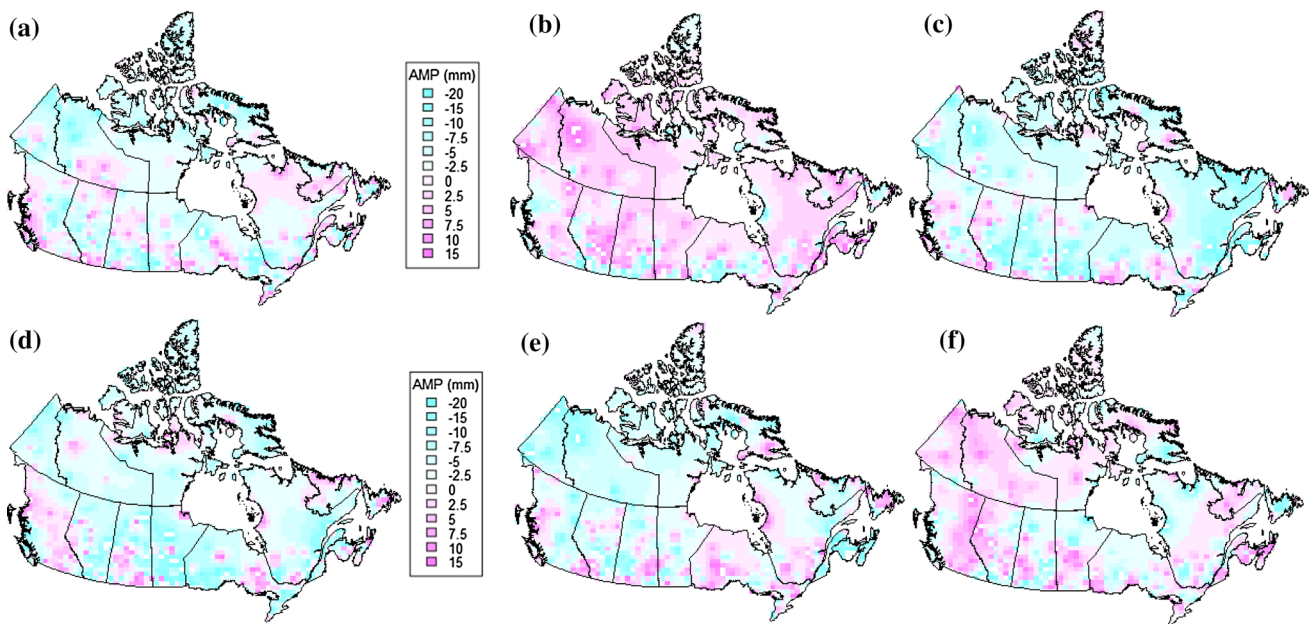


Fig. 6 The spatial distributions of differences in AMP of 20-year return period predicted by GEV distributions based on parameters estimated from the maximum and the minimum historical values of a given covariate. The respective covariate used was the year for (a), SOI for (b), Nino3 for (c), NAO for (d), PDO for (e), and NP for (f). The red (blue) grids means that the difference in AMP estimated from the GEV derived from the maximum covariate values are higher

(lower) than that derived from the minimum historical values of the covariate, and the gridded, difference in AMP values were interpolated from station AMP values by a simple Kriging method. The difference in AMP estimated from GEV distributions based on the maximum versus the minimum covariates such as El Niño or La Niña can exceed 20 mm

climate patterns on the spatial variations of Canadian AMP differs between the climate patterns, while Figs. 5a and 6a show temporal changes in AMP over the study period of each station. Even though there are minor differences between results derived from different periods, the overall significance of the relationships (Table 1; Figs. 5, S4 and S6) and their spatial distributions (Figs. 6, S5 and S7) are consistent.

Approximately 29.3 % of the AMP time series fitted to GEV distributions show significantly better fit to GEV distributions if the time was used as a covariate for the location parameter of GEV distributions. The proportion of AMP time series that fitted well to GEV distributions increased to about 33.9 % when the time was used as a covariate for both location and scale parameters for GEV distributions. Apparently, about 1/3 of AMP time series shows non-stationary characteristics. Stations that show significant increase in AMP of 20-year return period are mainly located in southwestern Canada, northern CP and Quebec (QC), Newfoundland (NL), and southwestern ON, while stations in southern CP, southeastern ON and Arctic region show significant decrease in AMPs of 20-year return period (Figs. 5a, 6a). Shook and Pomeroy (2012) also found that the single-day summer rainfalls had decreased at many locations in Southern CP over 1901–2000 and 1951–2000.

The effects of ENSO represented by SOI and NINO3 on AMP time series are shown in Figs. 5b, c and 6b, c where SOI and NINO3 were covariates for the location and scale parameters of GEV distributions fitted to Canadian AMP. Although only about 10.6 and 11.5 % (Table 1) of the GEV distributions fitted to AMP time series show significant improvement when SOI and NINO3 were used as covariates for the location parameter, respectively, according to results obtained from the Walker’s test and the false discovery rate (FDR) approach (Wilks 2006), the improvement is considered as field-significant across Canada. However, when SOI and NINO3 were incorporated as covariates to both the location and scale parameters of GEV distributions fitted to AMP time series, about 15.8 and 16.4 % of the GEV distributions show significant improvement, respectively, and so their improvements are also considered to be field-significant.

In Fig. 6c, areas colored pink (light green) are areas where a high NINO3 index means a wetter (drier) climate than a low NINO3 index, and vice versa. Therefore, a high NINO3 index (when El Niño is active) means that Canada will tend to be dry. In contrast, when NINO3 is low (which means when La Niña is active), Canada tends to be wet. As expected, Fig. 6b shows a more or less opposite pattern to Fig. 6c because when the SOI index is positive (negative), La Niña (El Niño) is active. However, there are minor

differences in AMPs of 20-year return period estimated from GEV distributions using either SOI or NINO3 as covariates to represent the effect of ENSO on the Canadian AMP (Figs. 5b, c, 6b, c). The influence of ENSO on the Canadian AMP represented shows more spatially consistent effect if SOI instead of NINO3 is used as the ENSO index.

The AMP of southwestern coastal areas, southern CP and the Great Lakes regions (light green area in Fig. 6b for SOI and the pink area in Fig. 6c for NINO3) tended to be higher in El Niño years than in La Niña years. Our results that AMP in the Great Lakes region during El Niño years tends to be high are consistent with that of Zhang et al. (2010) who found that extreme winter precipitation tends to be high during El Niño years. Because AMP in the Great Lakes region can occur either in summer or winter (Fig. S2), it seems the effects of ENSO on the extreme winter and summer precipitation of the Great Lakes region are similar to each other.

The AMP in central CP tends to be lower in El Niño than in La Niña years, which was in agreement with the higher winter total precipitation in La Niña than in El Niño years found by Shabbar et al. (1997) and Gan et al. (2007) for the southwestern Canada, including the CP. However, Zhang et al. (2010) found high extreme winter precipitation associated with El Niño for the central CP. Most northern Canada experienced inconsistent changes to AMP in El Niño than in La Niña years (Fig. 5b, c), which is different from the results of Zhang et al. (2010) who found that extreme winter precipitation in El Niño years was usually higher than that in the La Niña years. Differences between their results and ours are believed to be partly due to the much smaller number of stations used by Zhang et al. (2010) for representing northern Canada, and for comparing maximum winter precipitation instead of AMP since AMP can occur either in winter or summer in northern Canada (Fig. S1).

Compared to fitting AMP data to stationary GEV distributions (Table 1), more AMP time series show significantly better fit to GEV distributions if NAO was used as a covariate for the location parameter (14.7 %) or both the location and shape parameters (19.7 %) of GEV distributions. Such a level of improvements is field-significant which demonstrates the influence of NAO on some of the AMP of Canada. The spatial patterns of NAO effects are similar to those of ENSO. High AMP in BC (except its southwestern coastal region), central CP and eastern ON is related to the warm phase of NAO, in contrast to low AMP in most northern Canada, northern CP and western ON also during the warm phase of NAO (Figs. 5d, 6d). However, based on composite analysis and GEV modeling, Zhang et al. (2010) suggested no field-significant influence of NAO on the NA extreme winter precipitation. Bonsal and Shabbar (2008)

also found the effect of NAO on the Canadian total precipitation to be modest and restricted to northeastern regions where the warm phase of NAO is related to negative winter precipitation anomalies. Again, since AMP of Canada tends to occur in the summer, the influence of NAO on the AMP of Canada is not expected to be similar to its influence on the winter precipitation. For example, Coulibaly and Burn (2005) and Coulibaly (2006) found significant differences in the relationships between NAO and spring, summer or autumn precipitation and streamflow of Canada.

The effect of PDO on Canadian AMP is also field-significant, as 11.6 % (16.1 %) of AMP series fitted to GEV distributions are significantly improved if PDO is used as a covariate for the location (both location and scale) parameters of GEV distributions. In northwest Canada (the light green region in Fig. 6e), AMP tends to be high during the cold phase of PDO, but low during the warm phase of PDO. This agrees with the effects of PDO on the streamflow of northwest Canada found by St. Jacques et al. (2010, 2014). In contrast, the warm phase of PDO results in high AMP in ON, QC and western BC (pink region), but exerts both increasing and decreasing effects on the AMP of CP. Again, the relations between Canadian AMP and PDO are different from the relations between winter extreme precipitation and PDO, since Zhang et al. (2010) found that extreme winter precipitation of the CP and the Great Lakes tends to be lower during the cold phase than the warm phase of PDO. It is needed to further explore variations in seasonal relationships between extreme precipitation such as AMP and large-scale climate patterns.

NP seems to have more influence marginally on the location than both the location and scale parameters of GEV, for the percentage of stations that shows better fit to GEV distributions is 14.3 % if NP was only used to estimate the location parameter, compared to 13.6 % of stations showing better fit to GEV if NP was used to estimate both location and scale parameters. In contrast to the effect of PDO, the warm phase of NP primarily resulted in high AMP in Canada except in some local areas of CP and ON.

3.2 Modeling heavy precipitation clusters with poisson regression

Occurrences of heavy precipitation (larger than 95th percentile) presented in terms of the mean, variance and coefficient of dispersion (ratio between the variance and the mean) show a well-organized spatial pattern (Fig. 2), similar to that shown in Figs. 3 and 4. These three statistics decrease from north to south except in the southwestern coastal region where these values are very large. The CP has the lowest mean, variance and coefficient of dispersion, with a mean lower than 5 days, a variance lower than 3 days, and a coefficient of dispersion lower than 2.0, while

northern Canada has the highest variance (>4.0 days) and the coefficient of dispersion (>2.5). For the mean counts of heavy precipitation, the spatial pattern in Northern Canada is less consistent since stations show a mix of high and low mean count values. 80.3 % stations have a coefficient of dispersion statistically significantly >1, except for some stations in the CP and the southern border of Canada. These over-dispersion characteristics indicate that Canadian heavy precipitation exhibits temporal clustering or non-stationary behavior.

Out of 463 stations (Fig. 7b), only 32 stations show statistically significant change points in the occurrences of heavy precipitation. However, for these 32 stations, only 12 (1) stations show increasing (decreasing) trends before the change point and 2 (2) stations showed increasing (decreasing) trends after the change point occurred, while the remaining 18 stations show no trends either before or after the change point. The years the change point occurred are not spatially consistent. Given that change points were only detected in about 7 % of stations (<9 % of stations for the four periods studied), other than in southwestern Canada, abrupt changes to occurrences of heavy precipitation events in Canada are not field-significant.

In contrast, slowly varying trends in the occurrence of heavy precipitation events are field-significant across Canada as both the Walker's test and FDR approach rejected the joint, multiple-site null hypothesis ($\beta_1 = 0$) to be statistically significant. In the Poisson regression analysis, for stations without detected change points, statistically significant decreasing trends dominate over increasing trends (45.5 vs. 21.0 %), with trend magnitudes, β_1 (years) ranging from -0.062 to 0.021 . Most stations showing increasing trends are located in the southwestern, east coast, northern Arctic and northeastern CP, while decreasing trends are widespread in the CP, eastern and northern Canada (Fig. 7a). Results obtained from all the four-period analysis consistently demonstrated changing characteristics of the frequency of heavy precipitation over Canada. However, considerably fewer stations with short data record over 1970–2010 (55.1 %) and 1950–2010 (45.0 %) were identified with significant trends than those with long data record over 1930–2010 (67.8 %) and 1900–2010 (78.5 %) (Table 1). By averaging counts of heavy events across Canada, e.g., no consideration of the spatial variability of occurrences of heavy events, Zhang et al. (2001) found no monotonically increasing or decreasing trends in the annual counts of heavy precipitation events. However, they detected interdecadal variability in the heavy precipitation events of Canada.

Spatial distributions of positive/negative relationships between occurrences of heavy precipitation and climate indices are shown in Fig. 8. The influence of ENSO on occurrences of heavy precipitation (>95 percentile) is more

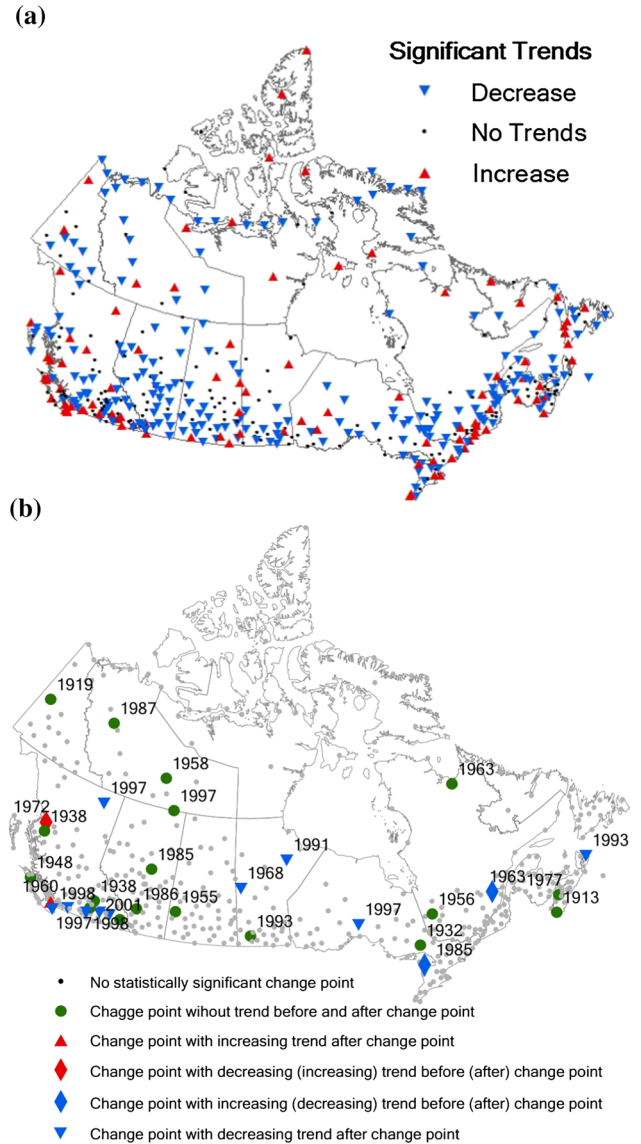


Fig. 7 Results of the fitting of the counts of heavy precipitation with a Poisson regression model with rate of occurrence that depends linearly on time (via a logarithmic link function) without (a) and with (b) a change point detected using the segmented regression. All change points and trends showing with green circles, red and blue triangles or diamonds are statistically significant at the 5 % significance level. The year when statistically significant change point occurred is numbered next to the station

significant than on the AMP time series because the number of stations (21.8 % for SOI and 21.0 % for NINO3, respectively; Table 1) with heavy precipitation significantly related to ENSO was almost 2 times of that of AMP. However, positive or negative influences of El Niño and La Niña on the occurrences of heavy precipitation are spatially consistent to that on AMP. For example, CP experiences more heavy precipitation in La Niña years than in El Niño years. Spatially, PDO exerts similar but more significant positive

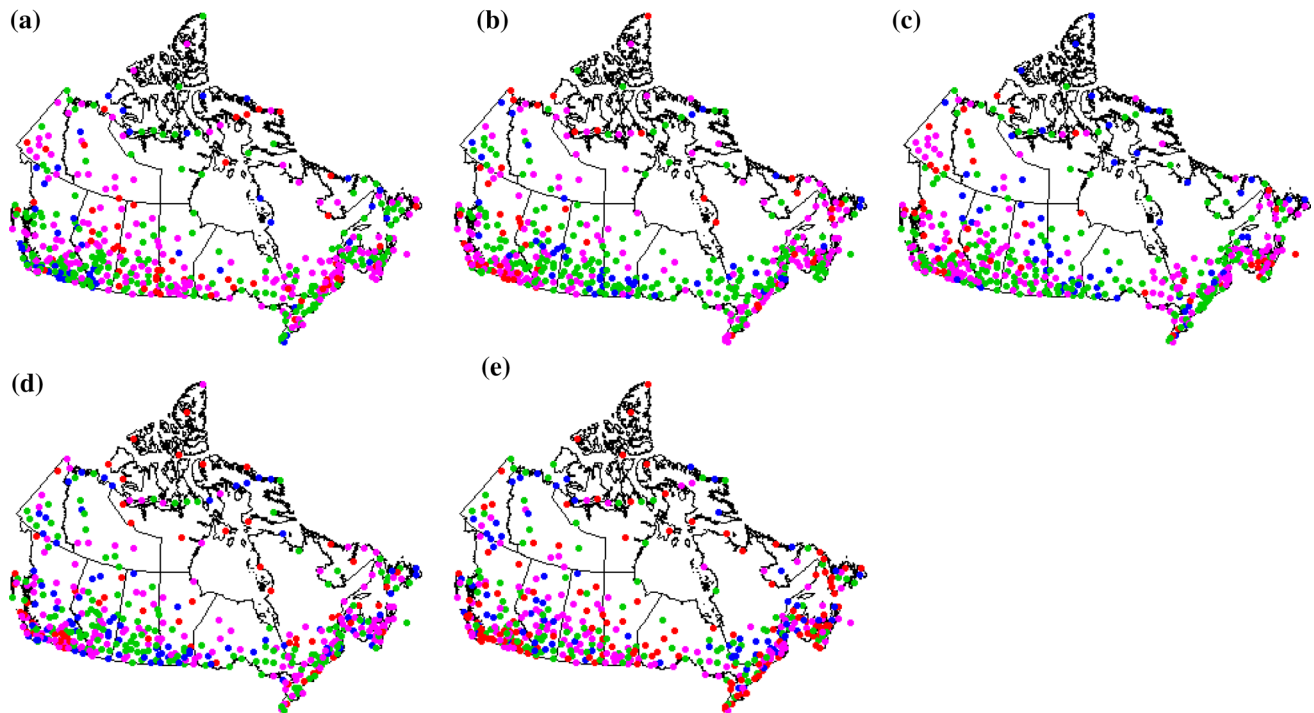


Fig. 8 Map showing the stations for which the five selected climate indices are covariates in the Poisson regression model. The red and magenta (blue and green) dots represent the positive (negative) relations between the rate of heavy precipitation occurrence and particu-

lar climate indices. Blue and red dots indicate stations whose Poisson regression modeling of the rate of heavy precipitation occurrence is significantly improved by implementing the covariates at the 5 % level. **a** SOI, **b** NINO3, **c** NAO, **d** PDO, **e** NP

or negative influences on occurrences of heavy precipitation than on AMP. NAO and NP also exert similar influences on occurrences of heavy precipitation and AMP across Canada.

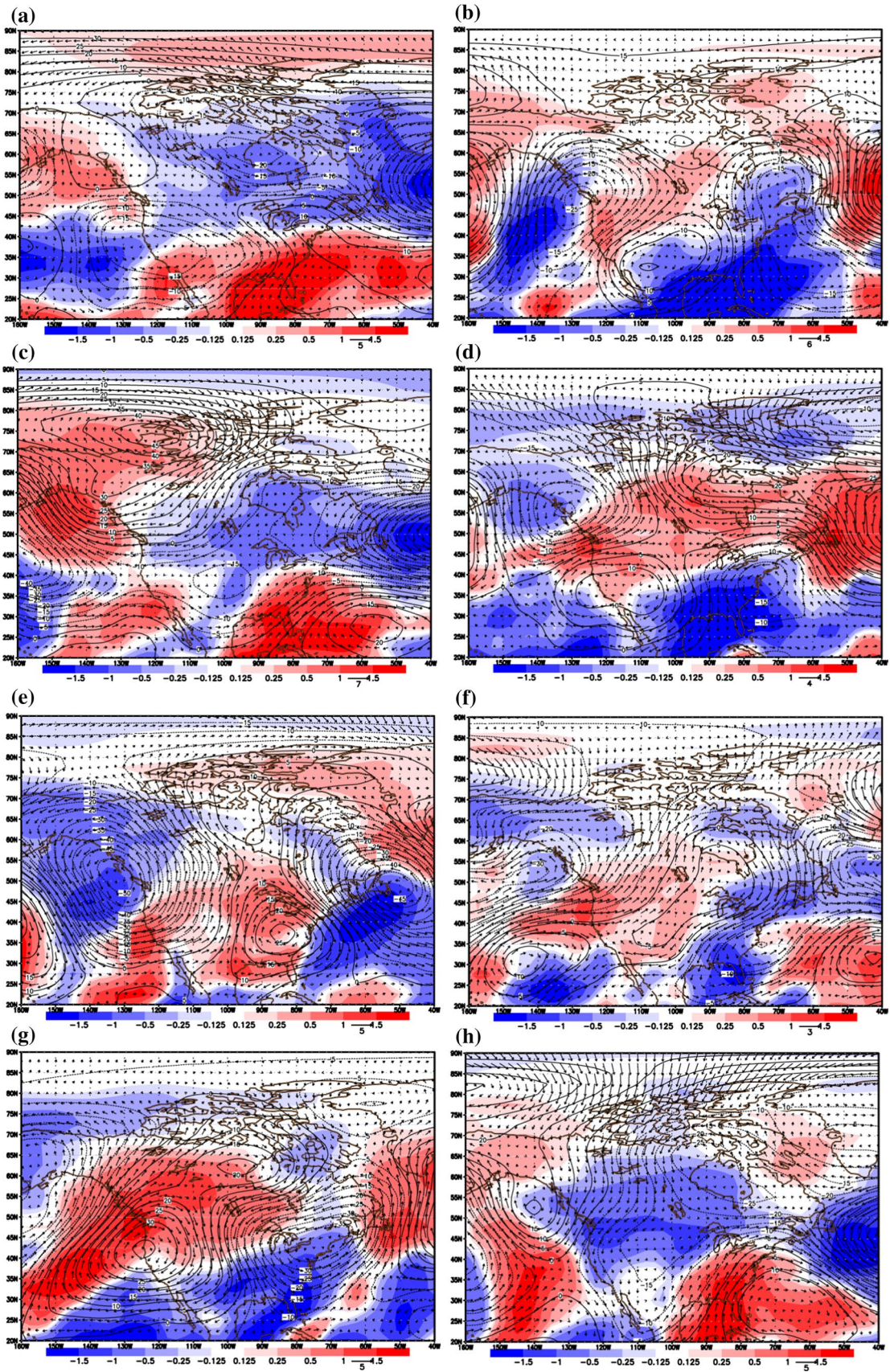
3.3 GP distribution

As a comparison, spatially distributed precipitation return levels of corresponding return periods were also calculated using a stationary GP model (Fig. 4d, f). Spatially, precipitation return levels increase in the north–south direction, and as expected, peaked in the southwestern and southeastern coastal regions of Canada, which is consistent with the location and scale parameters of GEV as shown in Fig. 3. Differences between precipitation return levels of 2-, 20- and 100-year return periods derived from GEV versus GP distributions are minor across Canada, except in the southwestern and eastern coastal areas, where GEV distributions estimate smaller extreme precipitation of the 2-, 20- and 100-year return period than GP distributions. For the above three return periods, overall GEV estimates precipitation return levels that are smaller than that of GP by about 8.0, 1.4 and 3.7 %, respectively.

Figure S3 shows the spatial distribution of signs (+ or –) of differences between precipitation return levels of 20-year

Fig. 9 Composite winter 500-hPa geopotential height (m; *contour with numbers*), 500-hPa wind field (m s^{-1} ; *vectors*) and vertically integrated precipitable-water-content (mm day^{-1} ; *shaded*) anomaly patterns for western Canada in winter days (Julian days 309–335) on which heavy precipitation most likely occurred, associated with **a** extreme El Niño (high NINO3), **b** extreme La Niña (low NINO3), **c** high PDO, **d** low PDO, **e** high NAO, **f** low NAO, **g** high NP and **h** low NP

return period estimated from GP distributions conditioned on positive and negative phases of selected climate indices used as covariates for scale parameters of GP distributions. The spatial relationships between AMP and covariates such as the time, SOI, NAO and PDO derived from GP distributions are similar to that derived from GEV distributions (Fig. 5). However, the scale parameter of GP distributions of many stations or the magnitude of AMP is significantly correlated with NINO3 and NP indices, which is different from that derived from GEV distributions. Because a fixed threshold was used in GP distributions, only the scale parameter of GP varies with time-varying covariates (climate indices). However, under the impact of a changing climate, the threshold value of GP can change more significantly than its scale parameter (Kysely et al. 2010; Sugahara et al. 2009). This is the reason that the GP distributions with only its scale parameter to be time-varying tends



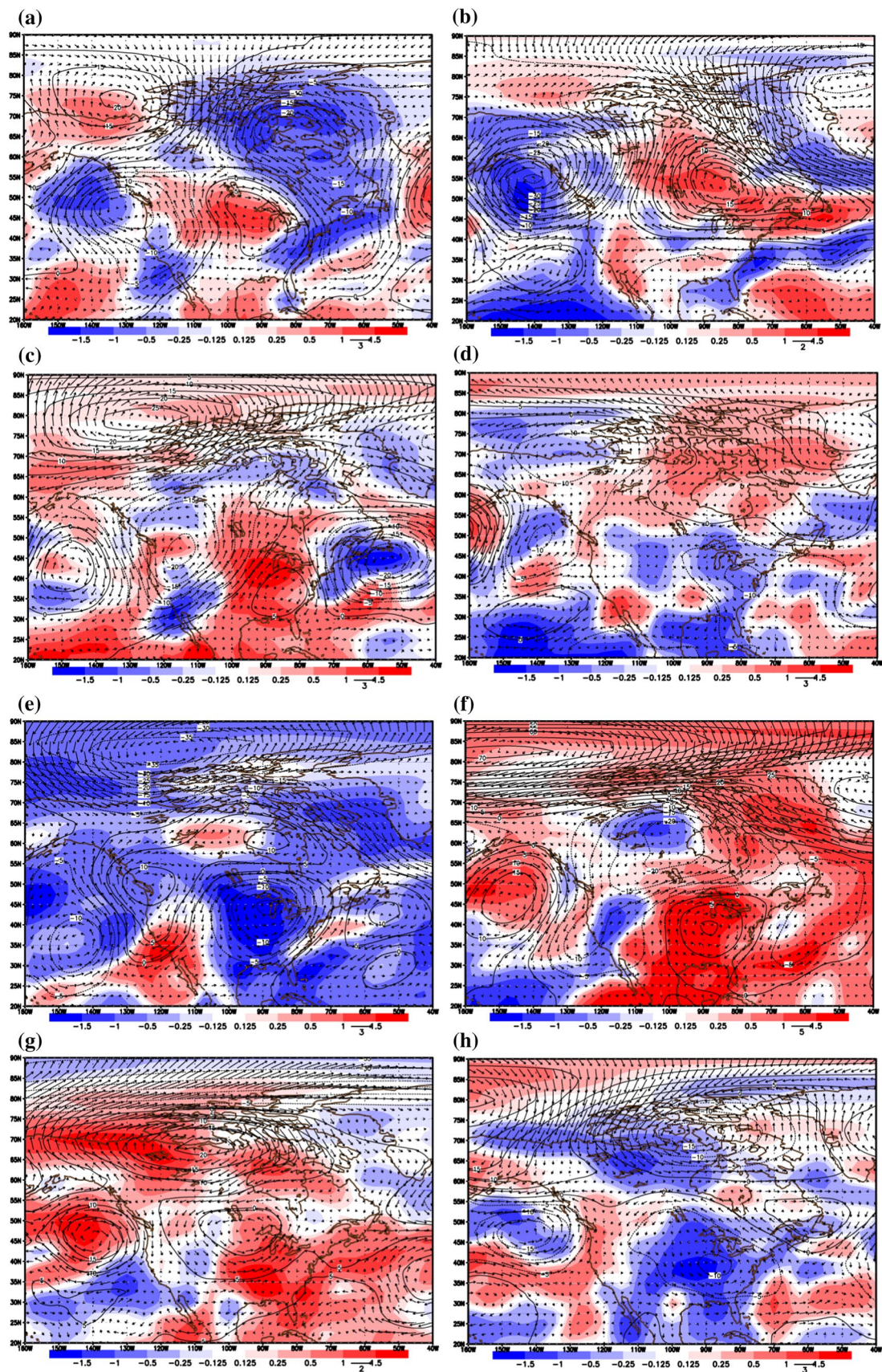


Fig. 10 Same as Fig. 9, but for western Canada in summer days (Julian days 184–227) on which heavy precipitation most likely occurred. **a** El Niño, **b** La Niña, **c** high PDO, **d** low PDO, **e** high NAO, **f** low NAO, **g** high NP and **h** low NP

to estimate lower precipitation return levels of 20-year return period for some stations during the warm phase of NP than GEV distributions with both time-varying location and scale parameters. Further studies should be conducted to examine the threshold of GP distributions related to time-varying climate indices. The high proportion of stations showing statistically significant correlation between the GP scale parameter and time-varying climate indices is strong evidence that extreme Canadian daily precipitation is non-stationary.

3.4 Composite circulation patterns

Because composite winter circulation anomaly patterns associated with heavy precipitation for western and eastern Canada are similar and have similar composite days (Julian days 309–335), only the winter patterns for western Canada are shown in Fig. 9. Composite analysis has advantage over the non-stationary extreme value analysis because the former separately investigates the influence of large-scale climate patterns on extreme summer and winter precipitation of Canada, while the latter is based on annual climate indices in which seasonal differences of large-scale climate patterns have been averaged out, which could decrease the statistical significance of extreme precipitation response to such climate patterns.

For total winter precipitation, Shabbar et al. (1997) found that strong El Niño episodes tend to associate with a deepened Aleutian low and an amplified western Canadian ridge which enhanced anticyclones and caused a northward shift of the mid-latitude jet stream, resulting in a drier southern Canada. On the other hand, La Niña winters are usually associated with an enhanced westerly flow, giving rise to more moisture in southern Canada. Wetter (drier) southern Canada in La Niña (El Niño) winters is also consistent with the positive (negative) PWC anomalies associated with La Niña (El Niño) (Fig. 9a, b). However, in central Canada, positive PWC anomalies are also associated with El Niño (Fig. S8a-b), and synoptic circulation patterns associated with heavy precipitation are likely more complicated than patterns associated with total winter precipitation found by Shabbar et al. (1997) because heavy precipitation involves higher spatiotemporal variabilities than total winter precipitation.

In western Canada, heavy precipitation that occur during El Niño winters tend to be relatively moderate because the lower branch of Pacific jet streams described by Shabbar et al. (1997) and Higgins et al. (2002) shifts north, thus missing western Canada (Fig. 9a), which is similar to circulation patterns giving rise to negative total winter precipitation anomaly in western Canada (Shabbar et al. 1997; Gan et al. 2007; Jiang et al. 2014). During La Niña winters, the subtropical Pacific jet stream (Higgins et al. 2002)

shift north, from southwestern (Fig. 9a) to the northwestern (Fig. 9b) United States, thus bringing positive heavy precipitation anomalies to western and central Canada. Heavy winter precipitation that occurs in central Canada during La Niña winters associated with deepened and northward shifted Aleutian Low (Fig. S8b) tend to be lower than heavy winter precipitation that occurs during El Niño winters associated with a normal and southeastward shifted Aleutian Low, positive geopotential heights, and intense polar jet streams (Fig. S8a). The above mechanism is in direct contrast to the mechanism behind that of total winter precipitation described in the previous paragraph.

In western Canada, summer days with heavy precipitation tend to be higher (lower) during El Niño (La Niña) years with positive (negative) moisture anomaly as shown in Fig. 10a, b, which agrees with the spatial pattern of AMP (see Fig. 6c) but in contrast to what was found by Shabbar and Skinner (2004). This is due to abundant moisture brought by the northeastward, subtropical jet stream to the western and central NA in El Niño summers (Figs. 10a, S9a). In La Niña summers, the deepened and southward shifted Aleutian low leads to positive wind anomalies to western Canada but that does not result in positive PWC anomalies for western Canada likely because of low moisture content in the north Pacific atmosphere (Fig. 10b). For eastern Canada, polar (North Atlantic) jet streams dominate El Niño (La Niña) summers (Figs. 10, S9 and S10), which result in negative (positive) PWC anomalies, which are consistent with low (high) AMP in eastern Canada during El Niño (La Niña) years (Fig. 6b, c).

The circulation patterns during active (inactive) PDO years are similar to that during El Niño (La Niña) years, but different in terms of the center location and strength of these circulation patterns, both during winters (Figs. 9 and S8) and summers (Figs. 10, S9 and S10), e.g., when PDO is inactive, the Aleutian Low (Figs. 9d and S8d) is shifted northward compared to when La Niña is active (Figs. 9b and S8b), which results in different spatial PWC anomalies between inactive PDO and La Niña winters. Bond and Harrison (2000) found that anomalously low (high) SST over the central North Pacific Ocean (west coast of Americas) typically occurs during active PDO winters. Active PDO leads to low pressure zones occurring over the North Pacific Ocean with enhanced anticlockwise winds, resulting in dry conditions in western Canada (Fig. 9c). In contrast, inactive PDO typically leads to wet conditions in western Canada. The influence of PDO on the heavy winter precipitation is similar to its influence on the winter total precipitation, of western Canada (Gan et al. 2007; Jiang et al. 2014; Mantua and Hare 2002).

Positive (negative) summer PWC anomalies (Figs. 10e, f, S9e-f and S10e-f) in northern Canada are associated with low (high) NAO. This pattern is similar to that of AMP

shown in Fig. 6d, which is likely caused by a shift in the direction of jet streams from the southwest during high NAO to northwest during low NAO between Arctic and North Atlantic. However, there are no consistent winter circulation anomaly patterns for NAO composites. The shift of the axis of maximum winter moisture from southwest to northeast across the Atlantic Ocean mainly affects the winter precipitation of northern Europe instead of NA (Hurrell and Van Loon 1997). Therefore, the correlation between NAO and Canadian extreme precipitation derived from the non-stationary analysis may be misleading as NAO index is the difference of atmospheric pressure at sea level between the Icelandic low located near Iceland and the Azores high located south of Canada.

A deepened and eastward shifted Aleutian Low during years of high NP index advects moist air towards the west coast of Canada, resulting in positive PWC anomalies (Figs. 9g, 10g, S9g and S10g) over western Canada. On the other hand, predominant wind patterns are in opposite directions during low NP years, resulting in typically negative PWC anomalies (Figs. 9h, 10h, S9h and S10h). These PWC anomalies derived from NP composite are consistent with composite differences of AMP shown in Fig. 6f. The impact of circulation patterns associated with the NP index on the heavy precipitation of Canada is similar to that of ENSO, because the inter-decadal variability of the northern Pacific described by the NP index are linked to the inter-annual variability of ENSO (Trenberth and Hurrell 1994). Even though ENSO, PDO and NP are all associated with the heavy precipitation of Canada, there are also local-scale synoptic processes that affect the heavy precipitation of Canada not accounted in our composite analysis of these climate anomalies. More detailed studies on circulation patterns associated with Canadian heavy and extreme precipitation should be conducted in the future.

4 Summary and conclusions

In this study, we have analyzed time series of AMP, POT and counts of extreme/heavy precipitation of 463 gauging stations of Canada using stationary and non-stationary GEV, GP distributions and Poisson regression, respectively. To create the non-stationary distributions, time-varying covariates that represent large-scale climate patterns such as ENSO, NAO, PDO and NP were incorporated to the location and scale parameters of GEV distributions, the rate of occurrence parameter of Poisson distributions and the scale parameter of GP distributions. To detect non-stationarities of Canadian extreme and heavy precipitation, we also used the time (year) as a covariate to estimate the parameters of non-stationary distributions.

Location and scale parameters of stationary GEV distributions fitted to the AMP data increase from north to south, and from inland to coastal regions of Canada. However, there was no clear spatial pattern for the shape parameters. Most stations had a non-zero shape parameter, which implies that most Canadian AMP series can be modeled by GEV Type II or Type III distributions with heavy tail behavior. Stationary GEV distributions estimated smaller extreme precipitation of the 2-, 20- and 100-year return period than stationary GP distributions by about 8.0, 1.4 and 3.7 %, respectively. In general, GEV distributions tend to under-estimate AMP of western and eastern coastal regions more than other regions of Canada. About 1/3 of the AMP time series shows non-stationary characteristics. Stations located in southwestern Canada, northern CP and QC, NL, and southwestern ON showed statistically significant increase in AMP, while AMP in southern CP, southeastern ON and Arctic region significantly decreased.

By using time-varying, climate indices as covariates in Poisson regression distributions, the results show that clusters of heavy precipitation events in Canada are related to large-scale climate patterns. The strength of storm clusters decreases spatially from north to south, but trends and abrupt changes to occurrences of the heavy precipitation appear to be less spatially consistent. By modeling AMP time series with non-stationary GEV and heavy precipitation with non-stationary GP distributions, it is evident that AMP and heavy precipitation of Canada show strong non-stationarities which are likely related to the influence of large-scale climate patterns given strong correlations are found between extreme Canadian precipitations and climate indices. AMP in southwestern coastal regions, southern CP and the Great Lakes regions tend to be higher in El Niño years than in La Niña years, while other regions of Canada showed a lower AMP in El Niño years than in La Niña years. The effect of other climate patterns such as PDO, NAO and NP on extreme precipitation is also significant in some stations across Canada. Given the influence of climate patterns on extreme precipitation of Canada is the primary focus of this study, future studies should focus on expected changes in Canadian extreme and heavy precipitation resulting from changes in large-scale climate patterns due to anthropogenic climate change.

Acknowledgments The authors thank the two anonymous reviewers for their constructive suggestions which significantly improved the paper. The first author was partly funded by the Chinese Scholarship Council (CSC) of China, and by the University of Alberta. We are grateful to Éva Mekis from Climate Research Division Environment Canada for providing us the precipitation data use in this study.

Appendix 1: GEV distribution

Let $M = \max \{Z_1, \dots, Z_n\}$ for large n , where Z_1, Z_2, \dots is a sequence of independent (or weakly dependent) identically distributed observations. In this study, Z_t represents daily observed precipitation recorded at a particular station on day t , and M is the AMP. Asymptotic results state that under some regularity conditions, normalizing sequences $\{a_n\}$ and $\{b_n > 0\}$ can be found such that (Coles 2001):

$$\Pr \left(\frac{M - a_n}{b_n} \leq y \right) \rightarrow \text{GEV}(y) \tag{1}$$

as $n \rightarrow \infty$, for a non-degenerate distribution function, which is the GEV distribution with the cumulative distribution function:

$$\text{GEV}(y; \mu, \sigma, \xi) = \begin{cases} \exp \left\{ - \left[1 + \xi \frac{y - \mu}{\sigma} \right]^{-1/\xi} \right\} & \xi \neq 0 \\ \exp \left[- \exp \left(\frac{y - \mu}{\sigma} \right) \right] & \xi = 0 \end{cases} \tag{2}$$

where $1 + \xi(y - \mu)/\sigma > 0$, μ, σ and ξ are the location, scale, and shape parameters, respectively. The shape parameter ξ determines the type of tail behavior. $\xi < 0$, $\xi = 0$ and $\xi > 0$ correspond to the Weibull (Type III), Gumbel (Type I) and Fréchet (Type II) distributions, respectively.

For a non-stationary process, the time-varying GEV parameters can be estimated by time-varying covariates. For instance, the GEV location parameter is defined through a linear function of covariates:

$$\mu = \beta X = \beta_0 + \beta_1 x_1 + \dots + \beta_m x_m \tag{3}$$

where $X = (1, x_1, \dots, x_m)$ is a matrix of the time-varying covariate vectors x_1, \dots, x_m , $\beta = (\beta_0, \beta_1, \dots, \beta_m)$ is the parameter vector to be estimated, in which β_0 is the intercept and β_1, \dots, β_m are the regression coefficients for the corresponding covariates; m is the number of covariates considered. The scale and shape parameters of the GEV distribution can be similarly expressed as Eq. (3).

Appendix 2: Poisson regression

The numbers of days (counts) of extreme values exceeding a threshold over a specified time interval (a year in this study) can be modeled by a Poisson distribution with an equal-dispersion (the mean equals the variance). However, the variance of observed data tends to be larger than the mean, known as over-dispersion, which can partly be attributed to the effect of temporal clustering (Mallakpour and Villarini 2015; Pinto et al. 2013; Villarini et al. 2011, 2013). The statistical significance of dispersion coefficients different from unity at 5 % significance level can be tested using the regression-based tests (Cameron

and Trivedi 1990) for testing over-dispersion in a Poisson model.

A Poisson regression models discrete data, in which the predict and follows a Poisson distribution. The counts in year i as N_i have a conditional Poisson distribution with the rate of occurrence parameter λ_i , given that:

$$P(N_i = k | \lambda_i) = \frac{e^{-\lambda_i} \lambda_i^k}{k!} \quad (k = 0, 1, 2, \dots) \tag{4}$$

where λ_i is a non-negative random variable. In a Poisson regression model, λ_i can be modeled as a function of predictors $x_{1i}, x_{2i}, \dots, x_{mi}$ in a manner similar to parameters of a non-stationary GEV (see Eq. 3):

$$\lambda_i = \exp (\beta_0 + \beta_1 x_{1i} + \beta_2 x_{2i} + \dots + \beta_m x_{mi}) \tag{5}$$

where β_j is the coefficient for the j -th predictor (x_{ji}) estimated by the maximum likelihood method. If β_j estimated is non-zero at a 5 % significance level, then there is a statistically significant relationship between the occurrence of extreme events and the predictor x_j . By relating λ_i to the time using an exponential function $\lambda_i = \exp (\beta_0 + \beta_1 i)$, changes in the mean number of occurrences of heavy precipitation with time can be examined. If β_1 is non-zero at the 5 % significance level, temporal changes in the mean number of extreme events are statistically significant (Villarini et al. 2011, 2012, 2013). The abrupt change points of the occurrences of extreme events can be further identified by a segmented regression in which the relation between the predictand and the predictor is piecewise linear. We used the function *segmented* in the R package ‘segmented’ (Mugge 2003) to detect change points and to estimate β_0 and β_1 for the Poisson regression model.

Appendix 3: GP distribution

The exceedance, $Q = Z - u$ (where Z is the observed precipitation and u the threshold) can be modeled as a GP distribution (Coles 2001):

$$\Pr (Q \leq q | Z > u) = GP_{\sigma, \xi}(q) = \begin{cases} 1 - \exp [-q/\sigma] & \xi = 0 \\ 1 - [1 + \xi q/\sigma]^{-1/\xi} & \xi \neq 0 \end{cases} \tag{6}$$

For $q \geq 0$ and $1 + \xi q/\sigma > 0$, where σ and ξ are the scale and shape parameters of a GP distribution. For $\xi = 0$, GP reduces to an exponential distribution. The GP distribution can be set up to model non-stationary processes, usually by making the scale parameter σ depend on particular covariate(s) (Coles 2001; Khaliq et al. 2006). The log of σ is regressed against covariates X , $\log (\sigma) = \beta X$, as shown in Eqs. 3 and 5.

The return level y_l is exceeded on average l times over a fixed period. Since there are on average λ peaks in the whole time series, the probability that an arbitrary peak exceeds y_l equals l/λ . Thus, y_l is obtained by adding the threshold to the $(1 - l/\lambda)$ quantile of the excess distribution (Coles 2001):

$$y_l = u + GP_{\sigma, \xi}^{-1}(1 - l/\lambda) = \begin{cases} u + \sigma \ln(l/\lambda) & \xi = 0 \\ u + \frac{\sigma}{\xi} \left[1 - \left(\frac{l}{\lambda} \right)^{-\xi} \right] & \xi \neq 0 \end{cases} \quad (7)$$

For presentation, it is often more convenient to give return levels on an annual scale, so that the N -year return level is the level expected to be exceeded once every N years.

Appendix 4: The likelihood-ratio test

The likelihood-ratio test can compare results obtained from GEV and GP distributions of parameters expressed with covariates of various complexities, such that the base covariate (e.g., M_0) is a subset of a more complex covariate (e.g., M_1). The likelihood-ratio test can determine which sets of model parameters will lead to the overall best model performance for GEV and GP. Suppose a base model M_0 is nested within a model M_1 , and L_0 (L_1) is the negative log-likelihood value for M_0 (M_1), then a deviance statistics is given by (Coles 2001):

$$D = -2(L_1 - L_0) \quad (8)$$

Large values of D indicate that M_1 is more adequate for representing the data than its base counterpart M_0 . The D statistic follows a Chi square distribution with degree of freedom, ν (difference between the number of parameters of the models M_0 and M_1). D_α is the $(1 - \alpha)$ quantile of the Chi square distribution at the α significant level. The null hypothesis $D = 0$ is rejected if $D > D_\alpha$. We used functions in the R package ‘extRemes’ (Gilleland and Katz 2011) for inferring the parameters of GEV and GP distributions and testing the significance of the relations between parameters and covariates.

References

- Ahmari H, Blais E-L, Greshuk J (2015) The 2014 flood event in the Assiniboine River Basin: causes, assessment and damage. *Can Water Resour J*. doi:10.1080/07011784.2015.1070695
- Alexander LV et al (2006) Global observed changes in daily climate extremes of temperature and precipitation. *J Geophys Res* 111:D05109. doi:10.1029/2005JD006290
- Allan RP, Soden BJ (2008) Atmospheric warming and the amplification of precipitation extremes. *Science* 321:1481–1484
- Blais E-L, Greshuk J, Stadnyk T (2015) The 2011 flood event in the Assiniboine River Basin: causes, assessment and damages. *Can Water Resour J*. doi:10.1080/07011784.2015.1046139
- Bond NA, Harrison DE (2000) The Pacific decadal oscillation, air–sea interaction and central north Pacific winter atmospheric regimes. *Geophys Res Lett* 27:731–734
- Bonsal B, Shabbar A (2008) Impacts of large-scale circulation variability on low streamflows over Canada: a review. *Can Water Resour J* 33:137–154
- Burn DH, Taleghani A (2013) Estimates of changes in design rainfall values for Canada. *Hydrol Process* 27:1590–1599
- Buttle JM, Allen DM, Caissie D, Davison B, Hayashi M, Peters DL, Pomeroy JW, Simonovic S, St-Hilaire A, Whitfield PH (2016) Flood processes in Canada: regional and special aspects. *Can Water Resour J*. doi:10.1080/07011784.2015.1131629
- Cameron AC, Trivedi PK (1990) Regression-based tests for overdispersion in the poisson model. *J Econom* 46:347–364
- Coles S (2001) An introduction to statistical modeling of extreme values. Springer, London
- Coulibaly P (2006) Spatial and temporal variability of Canadian seasonal precipitation (1900–2000). *Adv Water Resour* 29:1846–1865
- Coulibaly P, Burn DH (2005) Spatial and temporal variability of Canadian seasonal streamflows. *J Clim* 18:191–210
- Environment Canada (2014) Canada’s top ten weather stories for 2013. <http://www.ec.gc.ca/meteo-weather/default.asp?lang=5En&n55BA5EAFC-1>
- Franzke CL (2013) Persistent regimes and extreme events of the North Atlantic atmospheric circulation. *Philos Trans A Math Phys Eng Sci* 371:20110471
- Gan TY, Gobena AK, Wang Q (2007) Precipitation of southwestern Canada: wavelet, scaling, multifractal analysis, and teleconnection to climate anomalies. *J Geophys Res* 112:D10110. doi:10.1029/2006JD007157
- Gilleland E, Katz RW (2011) New software to analyze how extremes change over time. *Eos Trans Am Geophys Union* 92(2):13–14
- Government of Alberta (2014) Alberta 2013–2014 flood recovery update. <http://alberta.ca/Flood-recovery-update.cfm>
- Groisman PY et al (1999) Changes in the probability of heavy precipitation: important indicators of climatic change. *Clim Change* 42:243–283
- Higgins RW, Leetmaa A, Kousky VE (2002) Relationships between climate variability and winter temperature extremes in the United States. *J Clim* 15:1555–1572
- Hurrell JW, Loon HV (1997) Decadal variations in climate associated with the North Atlantic oscillation. *Clim Change* 36:301–326
- Jiang R, Gan TY, Xie J, Wang N (2014) Spatiotemporal variability of Alberta’s seasonal precipitation, their teleconnection with large-scale climate anomalies and sea surface temperature. *Int J Climatol* 34:2899–2917
- Kalnay E et al (1996) The NCEP/NCAR 40-year reanalysis project. *Bull Am Meteorol Soc* 77:437–471
- Kenyon J, Hegerl GC (2008) Influence of modes of climate variability on global temperature extremes. *J Clim* 21:3872–3889
- Khaliq MN, Ouarda TBMJ, Ondo JC, Gachon P, Bobée B (2006) Frequency analysis of a sequence of dependent and/or non-stationary hydro-meteorological observations: a review. *J Hydrol* 329:534–552
- Kunkel KE (2003) North American trends in extreme precipitation. *Nat Hazards* 29:291–305
- Kunkel KE, Andsager K (1999) Long-term trends in extreme precipitation events over the conterminous United States and Canada. *J Clim* 12:2515–2572
- Kuo C-C, Gan TY, Gizaw M (2015) Potential impact of climate change on intensity duration frequency curves of central Alberta. *Clim Change* 130:115–129

- Kyselý J, Pícek J, Beranová R (2010) Estimating extremes in climate change simulations using the peaks-over-threshold method with a non-stationary threshold. *Global Planet Change* 72:55–68
- Mailhot A, Kingumbi A, Talbot G, Poulin A (2010) Future changes in intensity and seasonal pattern of occurrence of daily and multi-day annual maximum precipitation over Canada. *J Hydrol* 388:173–185
- Mailier PJ, Stephenson DB, Ferro CAT (2006) Serial clustering of extratropical cyclones. *Mon Weather Rev* 134:2224–2240
- Mallakpour I, Villarini G (2015) The changing nature of flooding across the central United States. *Nat Clim Change* 5:250–254
- Mantua NJ, Hare SR (2002) The Pacific decadal oscillation. *J Oceanogr* 58:35–44
- Mantua NJ, Hare SR, Zhang Y, Wallace JM, Francis RC (1997) A Pacific interdecadal climate oscillation with impacts on salmon production. *Bull Am Meteorol Soc* 78:1069–1079
- Maraun D, Rust HW, Osborn TJ (2010) Synoptic airflow and UK daily precipitation extremes. *Extremes* 13:133–153
- Mekis É, Hogg WD (1999) Rehabilitation and analysis of Canadian daily precipitation time series. *Atmos Ocean* 37:53–85
- Mekis É, Vincent LA (2011) An overview of the second generation adjusted daily precipitation dataset for trend analysis in Canada. *Atmos Ocean* 49:163–177
- Milrad SM, Gyakum JR, Atallah EH (2015) A meteorological analysis of the 2013 Alberta Flood: antecedent large-scale flow pattern and synoptic-dynamic characteristics. *Mon Weather Rev* 143(7):2817–2841. doi:10.1175/mwr-d-14-00236.1
- Min S-K, Cai W, Whetton P (2013) Influence of climate variability on seasonal extremes over Australia. *J Geophys Res Atmos* 118:643–654
- Mladjic B, Sushama L, Khaliq MN, Laprise R, Caya D, Roy R (2011) Canadian RCM projected changes to extreme precipitation characteristics over Canada. *J Clim* 24:2565–2584
- Muggeo VM (2003) Estimating regression models with unknown break-points. *Stat Med* 22:3055–3071
- Newton B, Burrell BC (2015) The April–May 2008 flood event in the Saint John River Basin: causes, assessment and damages. *Can Water Resour J*. doi:10.1080/07011784.2015.1009950
- Peterson TC, Zhang X, Brunet-India M, Vázquez-Aguirre JL (2008) Changes in North American extremes derived from daily weather data. *J Geophys Res* 113:D07113. doi:10.1029/2007JD009453
- Pinto JG, Bellenbaum N, Karremann MK, Della-Marta PM (2013) Serial clustering of extratropical cyclones over the North Atlantic and Europe under recent and future climate conditions. *J Geophys Res Atmos* 118:12476–412485
- Pomeroy JW, Stewart RE, Whitfield PH (2015) The 2013 flood event in the South Saskatchewan and Elk River basins: causes, assessment and damages. *Can Water Resour J*. doi:10.1080/07011784.2015.1089190
- Rayner NA et al (2003) Global analyses of sea surface temperature, sea ice, and night marine air temperature since the late nineteenth century. *J Geophys Res Atmos* 108:4407. doi:10.1029/2002JD002670
- Ropelewski CF, Halpert MS (1986) North American precipitation and temperature patterns associated with the El Niño/Southern Oscillation (ENSO). *Mon Weather Rev* 114:2352–2362
- Ropelewski CF, Jones PD (1987) An extension of the Tahiti–Darwin southern oscillation index. *Mon Weather Rev* 115:2161–2165
- Saad C, St-Hilaire A, Gachon P, El Adlouni S (2015) The 2011 flood event in the Richelieu River basin: causes, assessment and damages. *Can Water Resour J*. doi:10.1080/07011784.2014.999825
- Seager R, Naik N, Vogel L (2012) Does global warming cause intensified interannual hydroclimate variability? *J Clim* 25:3355–3372
- Shabbar A, Skinner W (2004) Summer drought patterns in Canada and the relationship to global sea surface temperatures. *J Clim* 17:2866–2880
- Shabbar A, Bonsal B, Khandekar M (1997) Canadian precipitation patterns associated with the Southern Oscillation. *J Clim* 10:3016–3207
- Shang H, Yan J, Zhang X (2011) El Niño–Southern Oscillation influence on winter maximum daily precipitation in California in a spatial model. *Water Resour Res* 47:W11507
- Shook K, Pomeroy J (2012) Changes in the hydrological character of rainfall on the Canadian prairies. *Hydrol Process* 26(12):1752–1766. doi:10.1002/hyp.9383
- Sillmann J, Croci-Maspoli M, Kallache M, Katz RW (2011) Extreme cold winter temperatures in Europe under the influence of north Atlantic atmospheric blocking. *J Clim* 24:5899–5913
- St. Jacques J-M, Sauchyn DJ, Zhao Y. (2010) Northern Rocky Mountain streamflow records: global warming trends, human impacts or natural variability? *Geophys Res Lett* 37:6. doi:10.1029/2009GL042045
- St. Jacques J-M, Huang YA, Zhao Y, Lapp SL, Sauchyn DJ (2014) Detection and attribution of variability and trends in streamflow records from the Canadian Prairie Provinces. *Can Water Resour J* 39(3):270–284. doi:10.1080/07011784.2014.942575
- Stadnyk T, Dow K, Wazney L, Blais E-L (2015) The 2011 flood event in the Red River Basin: causes, assessment and damages. *Can Water Resour J* 1–9. doi:10.1080/07011784.2015.1008048
- Sugahara S, da Rocha RP, Silveira R (2009) Non-stationary frequency analysis of extreme daily rainfall in Sao Paulo, Brazil. *Int J Climatol* 29:1339–1349
- Szeto K, Brimelow JC, Gysbers P, Stewart RE (2015) The 2014 extreme flood on the southeastern Canadian prairies. *Bull Am Meteorol Soc* 96(12):520–552
- Tramblay Y, Neppel L, Carreau J, Najib K (2013) Non-stationary frequency analysis of heavy rainfall events in southern France. *Hydrolog Sci J* 58:280–294
- Trenberth KE (1997) The definition of El Niño. *Bull Am Meteorol Soc* 78:2771–2777
- Trenberth KE, Hurrell JW (1994) Decadal atmosphere-ocean variations in the Pacific. *Clim Dyn* 9:303–319
- Villarini G, Smith JA, Baeck ML, Vitolo R, Stephenson DB, Krajewski WF (2011) On the frequency of heavy rainfall for the Midwest of the United States. *J Hydrol* 400:103–120
- Villarini G, Smith JA, Serinaldi F, Ntelekos AA, Schwarz U (2012) Analyses of extreme flooding in Austria over the period 1951–2006. *Int J Climatol* 32:1178–1192
- Villarini G, Smith JA, Vecchi GA (2013) Changing frequency of heavy rainfall over the central United States. *J Clim* 26:351–357
- Vincent LA, Mekis É (2006) Changes in daily and extreme temperature and precipitation indices for Canada over the twentieth century. *Atmos Ocean* 44:177–193
- Wazney L, Clark SP (2015) The 2009 flood event in the Red River Basin: causes, assessment and damages. *Can Water Resour J*. doi:10.1080/07011784.2015.1009949
- Wilks DS (2006) On “field significance” and the false discovery rate. *J Appl Meteorol Clim* 45:1181–1189
- Zhang X, Vincent LA, Hogg WD, Niitsoo A (2000) Temperature and precipitation trends in Canada during the 20th century. *Atmos Ocean* 38:395–429
- Zhang X, Hogg WD, Mekis É (2001) Spatial and temporal characteristics of heavy precipitation events over Canada. *J Clim* 14:1923–1936
- Zhang X, Wang J, Zwiers FW, Groisman PY (2010) The influence of large-scale climate variability on winter maximum daily precipitation over North America. *J Clim* 23:2902–2915